Identifying patterns of spatial current dispersion that characterise and separate the Brugada syndrome and complete right-bundle branch block

A. Kandori[1] W. Shimizu[2] M. Yokokawa[2] T. Noda[2]
S. Kamakura[2] K. Miyatake[2] M. Murakami[3] T. Miyashita[1]
K. Ogata[1] K. Tsukada[1]

[1]Central Research Laboratory, Hitachi, Ltd, Tokyo, Japan
[2]National Cardiovascular Center, Osaka, Japan
[3]Hitachi High-Technologies, Ibaraki, Japan

Abstract—*The aim of the study was to detect patterns of spatial-current distribution in the late QRS and early ST-segments that distinguish Brugada-syndrome cases from complete right-bundle branch block (CRBBB). Magnetocardiograms (MCGs) were recorded from Brugada-syndrome patients ($n = 6$), CRBBB patients ($n = 4$) and the members of a control group ($n = 33$). The current distributions at six time points from Q-onset were estimated by producing current-arrow maps (CAMs). The angle of the current arrow of maximum amplitude at each time point was calculated. In the Brugada cases, the characteristic ST elevation was seen above the upper right chest, and abnormal currents appeared to be present in the right-ventricular outflow tract (RVOT). The angles of the abnormal arrows were $-78^\circ \pm 51^\circ$ at 100 ms and $-50^\circ \pm 61^\circ$ at 110 ms. In the cases of CRBBB, wide S- and R-waves were recorded above the upper right and lower right chest, respectively. The angles of the abnormal arrows for CRBBB were $152^\circ \pm 19^\circ$ at 100 ms, $159^\circ \pm 20^\circ$ at 110 ms, and $157^\circ \pm 19^\circ$ at 120 ms. The findings suggest that an abnormal current from the RVOT to the upper left chest may be a feature of the Brugada syndrome, and that the direction of this current is completely different from that seen in CRBBB.*

Keywords—*Brugada syndrome, Right-bundle branch block, Magnetocardiogram, Current-arrow map*

Med. Biol. Eng. Comput., 2004, **42**, 236–244

1 Introduction

THE BRUGADA syndrome is an electrical disorder of the heart that is associated with a high risk of sudden death (BRUGADA and BRUGADA, 1992; BRUGADA *et al.*, 2000*a*; IKEDA 2002). In particular, the pattern that characterises the syndrome consists of a right-bundle branch block (RBBB) with ST-segment elevation in the V1–V3 electrocardiograph (ECG) leads and a normal QT interval in the absence of structural heart disease (BRUGADA and BRUGADA, 1992).

Since the syndrome was identified, heterogeneous repolarisation across the ventricular wall of the right-ventricular outflow tract (RVOT) has been assessed as being responsible for the ST-elevation and genesis of ventricular fibrillation (VF) in several clinical and cellular studies (YAN and ANTZELEVITCH, 1990; MIYAZAKI *et al.*, 1996; MATSUO *et al.*, 1998; ANTZELEVITCH *et al.*, 1999; BRUGADA *et al.*, 2000*b*; SHIMIZU *et al.*, 2000*a*; *b*; KANDA *et al.*, 2002; KURITA *et al.*, 2002; MASAKI *et al.*, 2002, WILDE *et al.*, 2002; ANTZELEVITCH *et al.*, 2002). The high take-off angles of the ST segments seen in cases of the Brugada syndrome may simply be mimicking the RBBB pattern and have the same origin; this possibility was discussed in some of the cited works. However, this RBBB-like pattern may be due, at least in part, to early repolarisation of the RV epicardium rather than to blocking of conduction in the right bundle.

Furthermore, Shimizu *et al.* applied body-surface potential mapping (BSPM) to find that the ST-segment elevation 20 ms after the end of the QRS complex was localised below the parasternal second and third intercostal spaces (SHIMIZU *et al.*, 2000*b*). Bruns also used BSPM and found that changes to the ECG in the left precordial leads were reversed relative to the changes seen in the right precordial leads (BRUNS *et al.*, 2002). Although these findings have provided us with important, characteristic ECG signs of the Brugada syndrome, the mechanism responsible for the ST elevation has not yet been identified.

We have developed a magnetocardiogram (MCG) system that provides us with maps that reflect the current distribution in the heart. The Brugada syndrome is an electrical abnormality of the heart, and spatial current dispersion is a factor in many other

Correspondence should be addressed to Dr Akihiko Kandori; email: kandori@crl.hitachi.co.jp

Paper received 19 May 2003 and in final form 2 December 2003

MBEC online number: 20043862

Table 1 Magnetocardiographic and other characteristics of control-group members, patients with Brugada syndrome and CRBBB patients

Patient	Sex	Age, years	QRS, ms	RR, ms	QT, ms	QTc
Brugada syndrome						
1	F	23	87	840	379	414
2	M	27	103	1100	383	365
3	M	56	88	940	365	376
4	M	36	91	630	349	440
5	M	57	137	780	420	476
6	M	48	102	1060	412	400
Mean ± SD	F/M = 1/5	41 ± 15	101 ± 19	892 ± 178	385 ± 27	412 ± 41
CRBBB						
7	M	75	130	750	425	491
8	F	59	127	810	419	466
9	M	59	147	1400	493	417
10	F	70	133	815	435	482
Mean ± SD	F/M = 2/2	66 ± 8	134 ± 9	944 ± 306	443 ± 34	464 ± 33
Control group						
Mean ± SD	F/M = 17/16	32 ± 7	86 ± 8	959 ± 156	400 ± 30	411 ± 24

such abnormalities. We thus felt that it would be worthwhile to apply the MCG to find out whether or not current dispersion is involved in this case.

The MCG has the potential to obtain current distributions with a high spatial resolution, because other organs, such as the lungs and bones, produce much less interference than in the case of an ECG (HOSAKA and COHEN, 1976*a*), even though the contribution of volume currents to the total magnetic field is still significant at 0.28 (HOSAKA and COHEN, 1976*b*). Furthermore, a physical thorax phantom has been used to confirm that the current dipole estimated by one MCG system is accurate to within 9 ± 8 mm (PESOLA *et al.*, 1999). The low distortion of cardiac magnetic fields has also made it possible to measure fetal MCG signals (KARINIEMI, 1974). Furthermore, plots of the tangential components of the magnetic field (or the tangential vectors calculated from the normal components of a magnetic field) reflect the spatial distribution of cardiac current and show visible patterns of peaks immediately above electrically activated regions (HOSAKA and COHEN, 1976*a*; *b*; TSUKADA *et al.*, 1999; HORIGOME *et al.*, 1999).

Although a volume conductor and tissue anisotropy have an influence on the cardiac currents, this visualisation technique has provided a high detection rate in the diagnosis of ischaemic and arrhythmic heart diseases in adults (TSUKADA *et al.*, 2000*a*; *b*; YAMADA, *et al.*, 2001; 2002; KANDORI *et al.*, 2001*a*; *b*; 2002; SATO *et al.*, 2001; 2002; SHIONO *et al.*, 2002; KANZAKI *et al.*, 2003). In particular, spatial current distributions estimated from MCGs taken from adults with long-QT syndrome (LQTS) have led to a more accurate characterisation of this syndrome and revealed that it actually consists of two sub-types (KANDORI *et al.*, 2002).

We have now tried recording MCG signals from Brugada and complete-RBBB (CRBBB) patients as a way of clarifying the spatial mechanisms involved in the ST-elevation abnormality of the Brugada syndrome. We used our method of creating two-dimensional current-arrow maps (CAMs) to visualise the spatial current distributions.

2 Materials and methods

2.1 *Subjects*

The diagnosis of Brugada syndrome was based on typical ECG patterns (persistent or transient right-precordial ST-segment elevation, with or without an atypical right-bundle branch block) and clinical arrhythmic events (syncope, ventricular fibrillation, cardiac arrest). A 12-lead ECG from one patient (number 2; see Table 1), showing the typical 'coved' pattern of Brugada syndrome, is shown in Fig. 1. The pattern is obvious in the signals on the V1–V3 leads.

Magnetocardiographic and other data on the Brugada and CRBBB patients and normal control volunteers are listed in Table 1. There were six Brugada patients (41 ± 15 years old), four CRBBB patients (66 ± 8 years old) and 33 normal (control) subjects (32 ± 7 years old); none of the latter had a history of cardiac disease. All of the CRBBB patients and three of the Brugada-syndrome patients showed longer QRS intervals than the controls. On the other hand, the RR intervals, QT intervals and corrected QT intervals (QTc values) were not significantly different from the data on the control subjects. The QTc values were calculated from Bazett's formula ($QTc = QT/\sqrt{RR}$). Note that all of the data in Table 1 were obtained from MCG signals.

2.2 *Measurement of magnetocardiograms*

Magnetocardiogram signals for each patient were recorded above the chest, in the positions shown in Fig. 2*a*, over a period of 30 min. These signals were measured using a superconducting quantum interference device (SQUID) system* (KANDORI *et al.*, 2001*a*; *b*; 2002). This system has 64 coaxial gradiometers and was installed in a room magnetically shielded by a double layer of μ-metal. The gradiometer array is an 8×8 matrix on a flat plane with a pitch of 25 mm. Each sensor incorporates a first-order gradiometer, composed of coils on an 18 mm diameter bobbin with a 50 mm long baseline. The MCG signals were passed through an analogue bandpass filter (0.1–100 Hz) and an analogue notch filter (50 Hz) and then digitised at a sampling rate of 1 kHz by an AD converter mounted in a computer.

2.3 *Signal analysis*

To improve their signal-to-noise ratios (SNRs), the MCG waveforms of each patient and volunteer were averaged 20–30 times, with the R-wave peak as a trigger. Superpositions of the averaged waveforms from the 64 sensors (as shown in Figs. 3*b*, 4*b* and 5*b*) were used so that the Q onset, QRS end and T end could be visually determined by the identification of discontinuities in the overlapping waveforms. The QT intervals listed in Table 1 were calculated from these results. Although the ST elevation makes determining the QRS end somewhat imprecise, the most important time point in the analysis of spatial current distribution is the Q onset, which is clearly

*MC-6400, Hitachi, Ltd

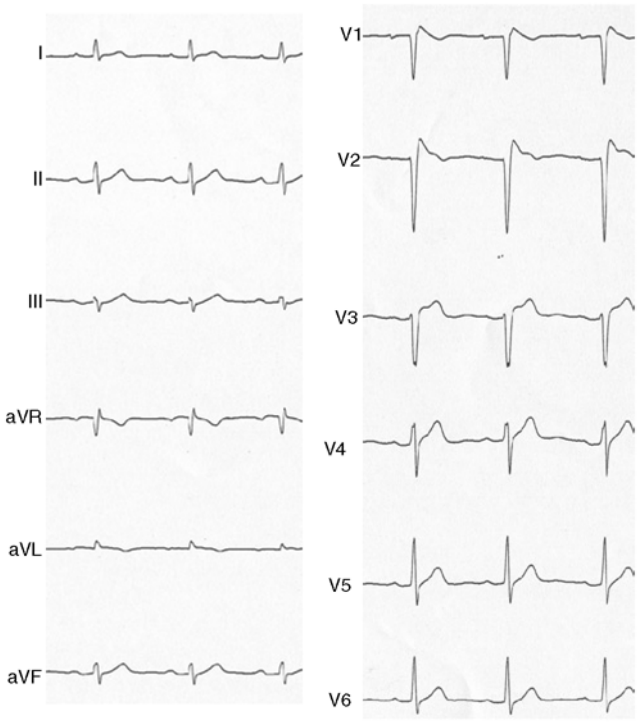

Fig. 1 *Typical 12-lead ECG waveform from patient with Brugada syndrome*

delineated. A base-line correction of the MCG signals was made by using the average magnetic field over the 20 ms before the onset of the Q-wave, because amplitude offsets in BSPM are, in general, correctable by subtracting the value in the PQ (BRUNS *et al.*, 2002). As such correction of the MCG can create problems when we take the spatial derivative (expressed in the following paragraph), we confirmed that the correction did not create problems with any of the data.

The main point of our arrayed MCG system is the production of CAMs from the derivatives of the normal components *Bz* of the individual MCG signals (KANDORI *et al.*, 2001*a*; *b*; 2002) by applying

$$Ix = \frac{dBz}{dy} \tag{1}$$

and

$$Iy = \frac{-dBz}{dx} \tag{2}$$

The magnitude of the current arrows ($I = (Ix^2 + Iy^2)^{1/2}$) is plotted as a contour map. We used spline interpolation to

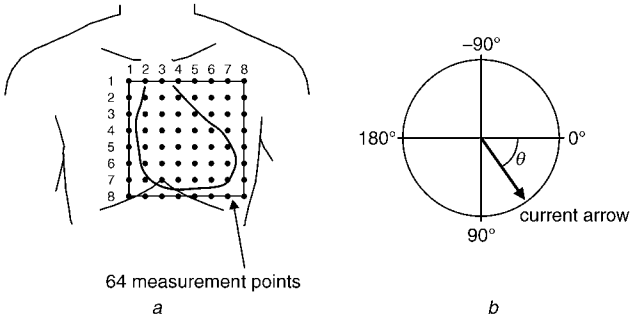

Fig. 2 *(a) MCG measurement area (8×8 matrix) above heart. Position of array is set by placing one sensor (column 7, row 3) above xiphoid sternum. (b) Angle θ of current arrow with maximum amplitude is defined in same way as electrical axis of an electrocardiogram*

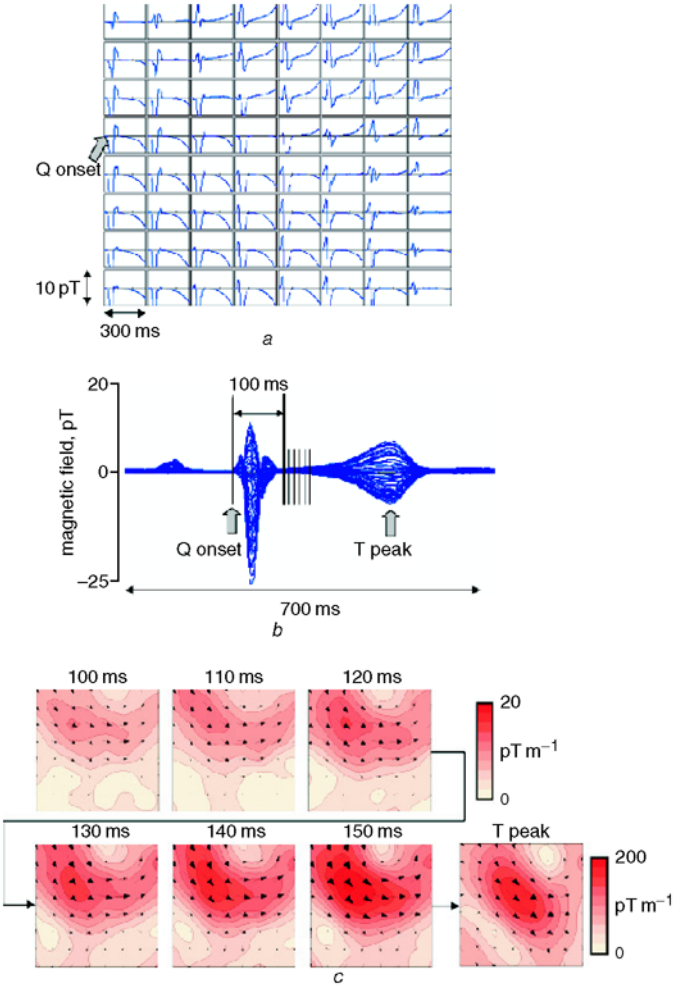

Fig. 3 *MCG results for typical, normal (control) subject: (a) 64 MCG waveforms, enlarged for identification of ST elevation; (b) superposition of 64 waveforms; (c) CAMs at six lines in ST-segment and peak position in T-wave of (b)*

obtain the data from which we obtained the current arrows in the measurement plane. Note that the current arrows produced using (1) and (2) do not exactly correspond to the physical current. However, the results of both simulation and measurement have shown a strong similarity between a current arrow thus derived and the actual tangential magnetic field in the corresponding region. The field corresponds to a local distribution of electrical current in which the components close to the surface make the strongest contribution, and so a current-arrow map is a very informative depiction of the spatial distribution of electrical activity near the relevant body surface.

The angle of the current arrow with maximum amplitude expresses an electrical axis (Fig. 2*b*) much the same as is commonly used in ECG study. In the case of ECG study, the axis reflects the main current orientation in the coronal plane, because the axis is obtained by integrating and obtaining a vector from two of the potentials (I and II), which run parallel to the *x*- and *y*-axis current components. This angle has been used to identify an abnormal current in the T-waves of LQTS patients (KANDORI *et al.*, 2002).

In this study, these angles were calculated for six positions (100, 110, 120, 130, 140 and 150 ms after the Q onset) in the late QRS or early ST-segment, because the elevation of the ST-segment 20 ms after the end of the QRS complex is the most characteristic ECG sign of the Brugada syndrome (SHIMIZU, 2000*b*). Furthermore, we set the start time at the Q onset because of the difficulty of determining the QRS end when the MCG data includes ST elevation.

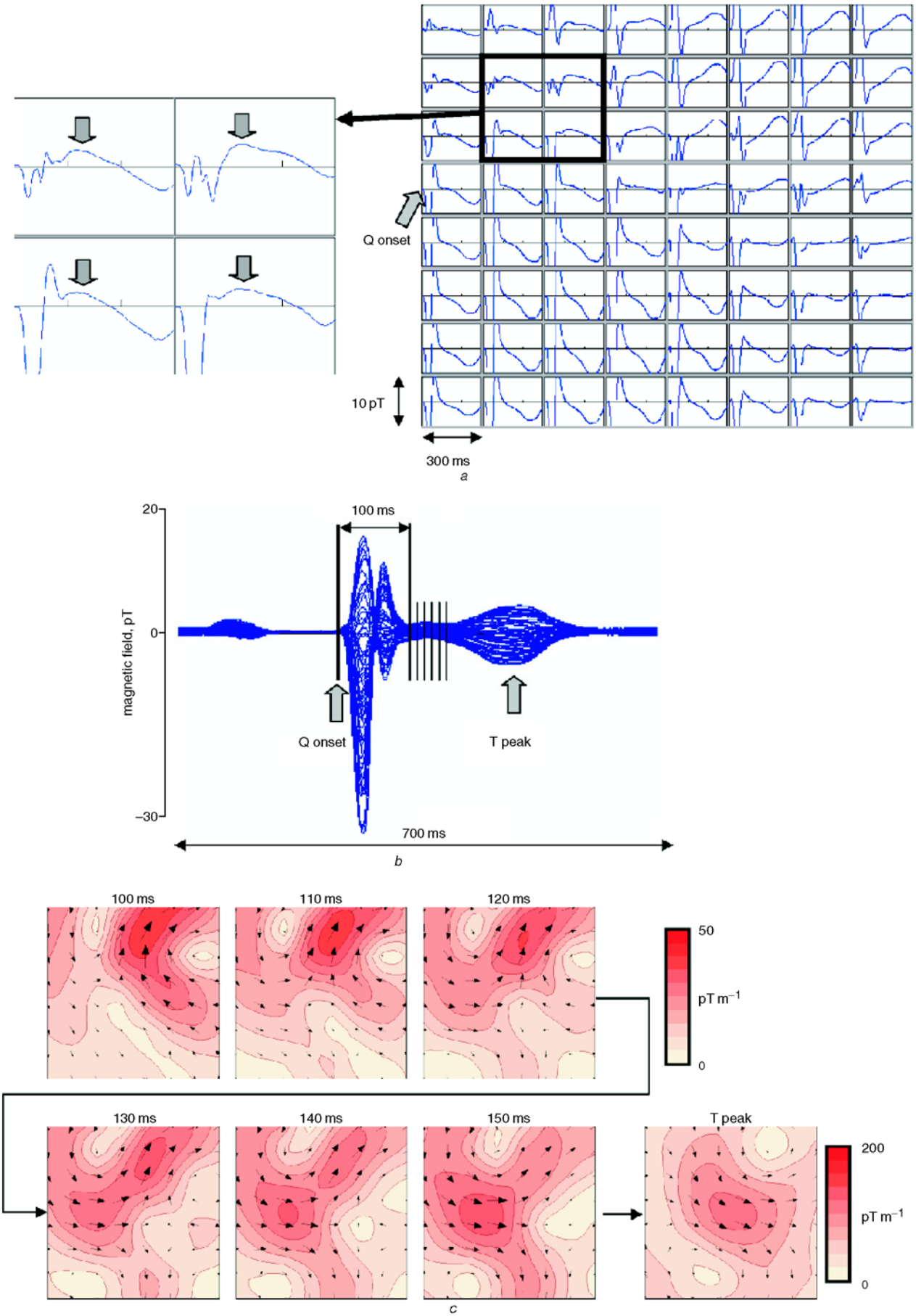

Fig. 4 *MCG results for typical patient with Brugada syndrome (patient 4 in Table 1): (a) on right, 64 MCG waveforms, with enlarged views on left to show typical ST elevation (coved and/or saddle-back type); (b) superposition of 64 waveforms; (c) CAMs at six lines in ST-segment and peak position in T-wave of (b)*

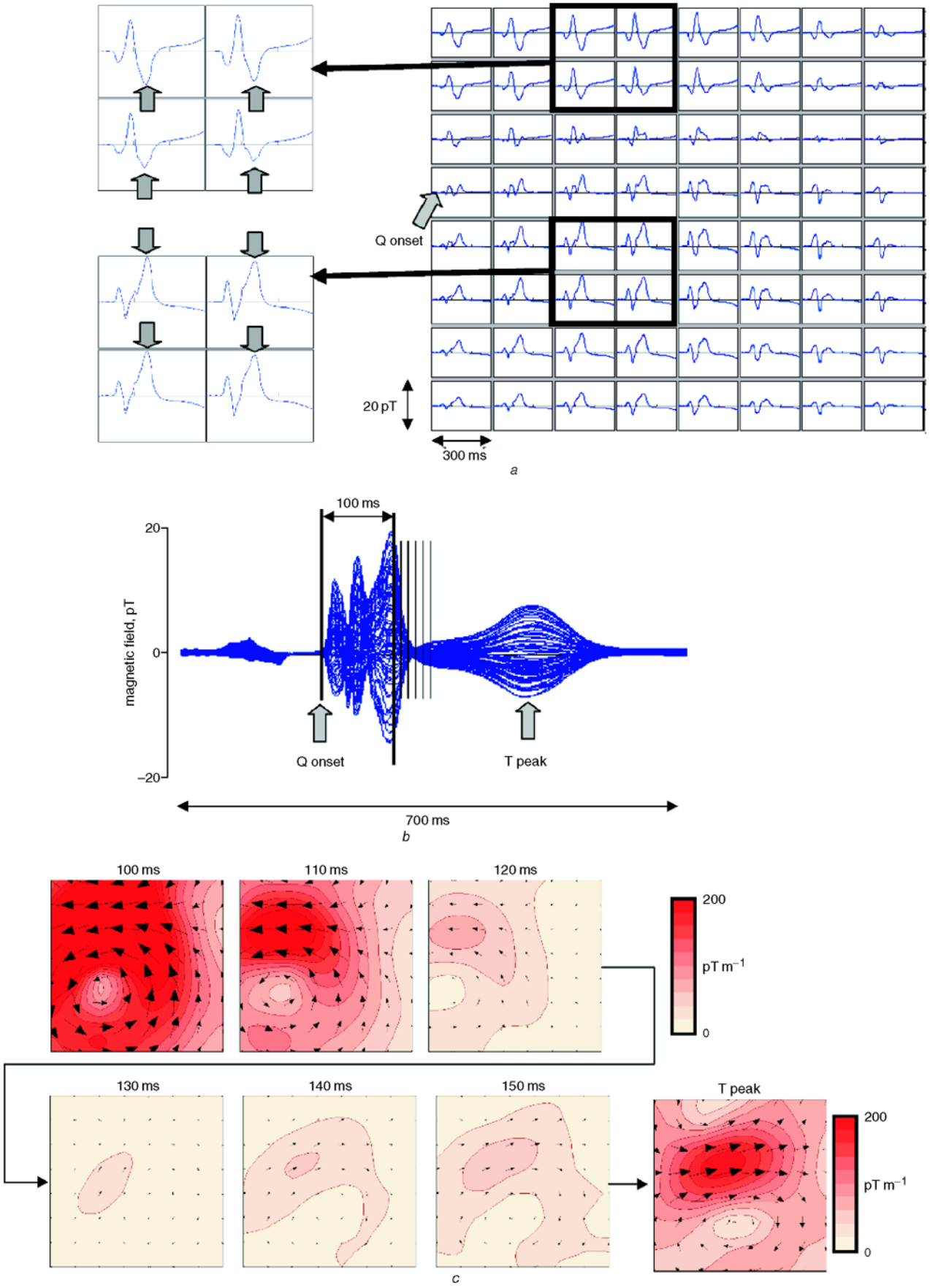

Fig. 5 *MCG results for typical patient with CRBBB (patient 7 in Table 1): (a) on right, 64 MCG waveforms, with enlarged views on left to show ST elevation (upper four graphs show typical, negative S-wave; lower four graphs show positive S-waves, with features of interest indicated by wide arrows); (b) superposition of 64 waveforms; (c) CAMs at six lines in late QRS complex and ST-segment and at peak position in T-wave of (b)*

3 Results

3.1 *MCG waveforms and CAM patterns of ST-segments in the control group*

The 64 averaged waveforms obtained in the plane above a typical subject from the normal control group are shown in Fig. 3*a*. In this Figure, we see neither ST elevation nor abnormal S-waves. The superposition of the 64 waveforms in Fig. 3*b* gives a precise view of the Q onset and T-wave peak (indicated by the wide arrows). We selected 100 ms after the Q onset as the starting point for arrow-map analysis. The QRS complex in this case is actually narrower than 100 ms; in fact, the average QRS width for the normal subjects was 86 ± 8 ms, as stated in Table 1.

Spatial current distributions, as evaluated using CAM, are shown in Fig. 3*c*; the corresponding positions are indicated in Fig. 3*b* by lines and the label 'T peak'. In the early phase of the ST-segment, the strongest current arrows appear near the upper right ventricle, and the position of the maximum moves lower during the ST-T activation.

3.2 *MCG waveforms and CAM patterns of the Brugada-syndrome patients*

Fig. 4*a* shows the 64 waveforms for a typical patient with the Brugada syndrome. ST elevation (coved and/or saddle-back type) is visible in many of the panels. This is particularly so of the upper-left sensor positions, four of which have been enlarged to provide a better view of their shapes. In Fig. 4*a*, however, it is difficult to discern the elevation, because its magnitude is very small (<3 pT), and the distinction between the saddle-back and coved types is not always clear, because the actual waveform is often a mix of the two types. Furthermore, it is difficult to provide quantitative data on the ST elevation, because the pattern of elevation differs from channel to channel, and it is difficult to define an appropriate time position for measurement. As well as the ST elevation, three of the Brugada-syndrome patients show QRS-complex durations that are significantly longer (103, 137 and 102 ms) than the average (86 ± 8 ms) for the normal control subjects, as is shown in Table 1. However, the Brugada-syndrome patients have disparate QRS intervals.

We obtained CAMs for these subjects, too, and the result is given in Fig. 4*c*. During the time interval from 100 to 120 ms, the strongest current arrows appear at an upper-central position that corresponds to the RVOT in all patients. At the first few time points, the larger arrows point upwards. A further set of strong-current arrows that point downwards and to the right, in a similar pattern to that seen in the normal control cases, start to appear and remain through the T-wave peak.

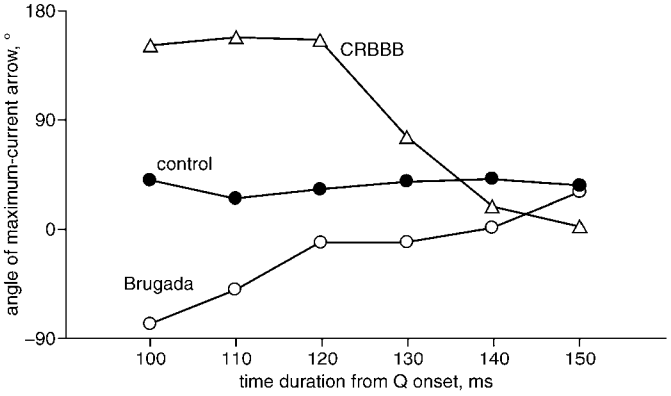

Fig. 6 *Relationship, for control subjects, Brugada-syndrome patients and CRBBB patients, of mean angle of maximum-current arrow at six positions (100, 110, 120, 130, 140 and 150 ms) in ST segment after Q onset. Values for (•) normal subjects, (○) Brugada-syndrome patients and (△) CRBBB patients. Differences between all three groups are large at 100 and 110 m*

3.3 *MCG waveforms and CAM patterns of CRBBB patients*

Fig. 5*a* shows the 64 waveforms for a typical patient with CRBBB. Large S- and R-waves are visible in the waveforms from the upper and lower sensors, respectively. The large amplitudes and long durations of these waves are seen in the eight enlargements on the left. The latter quality lengthens the QRS complex (Fig. 5*b* and the average value, 134 ± 9 ms, as given in Table 1). Therefore the position 100 ms after the Q onset is well within the QRS complex.

This characteristic of the waveforms means that the spatial distribution of current over the period from 100 to 120 ms reflects depolarisation activity. During this period, strong-current arrows pointing leftward appear above the upper-right ventricle (Fig. 5*c*). After this period, new strong-current arrows that point rightward appear and remain dominant through the T-wave peak.

3.4 *Quantitative evaluation of directions in the abnormal cases*

Mean values of the main current-arrow angle provide a way quantitatively to investigate the variation within the ST-segment and are plotted in Fig. 6 (mean values are drawn to avoid a

Table 2 Numerical results for angles of current arrows with maximum amplitude at six points in time: mean values (Fig. 5) and standard deviations

	Control group ($n = 33$)		Brugada syndrome ($n = 6$)		CRBBB ($n = 4$)
100 ms	40 ± 61	$p < 0.05$	-78 ± 51	$p < 0.05$	152 ± 19
110 ms	25 ± 62	$p < 0.05$	-50 ± 61	$p < 0.05$	159 ± 20
120 ms	32 ± 44	$p = 0.27$	-10 ± 82	$p < 0.05$	157 ± 19
130 ms	39 ± 39	$p = 0.19$	-10 ± 71	$p < 0.52$	76 ± 104
140 ms	41 ± 43	$p = 0.28$	1 ± 79	$p < 0.65$	18 ± 90
150 ms	35 ± 34	$p = 0.78$	31 ± 34	$p < 0.31$	2 ± 54

complicated Figure; although the variance is a little large, and the populations are small, separation of the data is clear). In normal subjects, there is little variation over the whole period. On the other hand, the plots for CRBBB and Brugada syndrome vary greatly within the same range. Furthermore, the difference between the directions for the two groups of patients is huge at 100 and 110 ms. Table 2 gives the relevant statistics. The angles at the beginning (100 and 110 ms) of the ST elevation (or late in the QRS) are significantly different for each of the three sets of subjects.

4 Discussion

4.1 *Mechanism behind ST elevation in the Brugada syndrome*

We have demonstrated the time-domain analysis and visual depiction of abnormal currents obtained from MCG signals as a step towards clarifying the mechanism behind ST elevation in cases of Brugada syndrome.

In time-domain analysis of the MCG, we saw that the three Brugada-syndrome subjects had longer QRS widths (103, 137 and 102 ms) than those (86 ± 8 ms) for the normal (control) subjects, whereas the QT and QTc intervals were not significantly different. The long mean QRS duration (101 ± 19 ms) at rest in the present study is similar to that (96 ± 10 ms) seen in the non-fibrillating Brugada-syndrome patients in one comparative ECG study (KANDA *et al.*, 2002). The lack of a difference in the QT interval reinforces similar characterisations from ECG findings (BRUGADA and BRUGADA, 1992). Furthermore, the ST-segments of the MCG waveforms were elevated, although at a low amplitude (<3 pT), and had shapes of the coved and/or saddle-back type above the upper right chest. Therefore the signs of the Brugada syndrome in MCG waveforms are a slightly broadened QRS complex and a small but significant ST elevation in the signals obtained from the sensors above the upper right chest.

To investigate the spatial current distribution that causes the ST elevation seen in the Brugada syndrome, the CAMs in Fig. 4 were produced from the signals during the period (100, 110, 120, 130, 140 and 150 ms) that is mainly characterised as the ST-segment. Although the period can also include a late QRS complex because of the difficulty of selecting a point as the QRS end (so that we may not have completely separated depolarisation and repolarisation), we are interested in the variation of current over time and the ST elevation in the Brugada syndrome, and so a reasonable approximation will suffice. During the period of ST elevation, abnormal current arrows are obtained above the positions in the upper central chest that correspond to the RVOT in all patients.

The main direction of the abnormal current 100 ms after the Q onset was $-78°$ (Table 2). The angle indicates current flow in almost the opposite direction to that seen in the normal case (40°). Experimental studies have suggested that the low ST elevation in the Brugada syndrome is caused by a loss of the action potential dome in the epicardial (Epi) cells but not in the endocardial (Endo) cells of the RVOT (YAN and ANTZELEVITCH, 1999). The opposite direction for the maximum-current arrow could indicate a current flow between Epi and Endo in the direction opposite to that which is normally seen. However, the maximum-current-arrow positions of the Brugada and control subjects are slightly different. Therefore the opposite current flow between Epi and Endo may not be the sole reason for the opposite direction of the maximum-current vector. However, these findings imply that the appearance of a negative angle (of about $-80°$) at around 100 ms is an indicator of the Brugada syndrome.

4.2 *Characteristics of CRBBB patients*

MCG waveforms of CRBBB patients feature long QRS complexes and large S- and R-waves. The large S- and R-waves appeared above the right-upper and -lower chest wall, respectively. Therefore the superposed CRBBB waveforms (Fig. 5*b*) show three clear phases (i.e. clear Q-, R- and S-waves) in the QRS complex, whereas the superposed waveforms (not presented here) of a patient with a complete left-bundle branch block (CLBBB) only show one phase. Thus the opposite polarity of the current angles in the late parts of the QRS complex in the CRBBB patients indicates the presence of a difference in flow angle, which depends on the direction of current flow between the R- and S-waves. In short, we can use the pattern of estimates of polarity to determine whether a patient has CRBBB or CLBBB. The flow from LV to RV is visible in the CAMs of Fig. 5*c*. The direction is reasonable if we consider the underlying electrophysiological phenomenon, because electrical activation in the ventricles propagates from left to right (i.e. blocking of the right bundle branch in cases of CRBBB cases means that the origin is the LV).

A model for the two-dimensional propagation of electrical activity in heart muscle has been investigated (ROBERGE *et al.*, 1986; DELGADO *et al.*, 1990). The model takes the muscle tissue as a network of cables, each representing a cell. Flows of intracellular current set up transmembrane currents. These results showed that the threshold requirement for active propagation is lower for transverse than for longitudinal propagation. The longitudinal direction of propagation coincides with current flowing in the direction of the gap-junction sequences.

Consequently, we can conclude that the pattern of MCG waveforms and the abnormal current direction seen in the CAM of six Brugada syndrome and four CRBBB patients may provide critical signs that allow us to identify Brugada-syndrome and CRBBB patients and to distinguish between the two.

4.3 *Comparison: results of MCG and BSPM for the Brugada syndrome*

We showed that the main direction of the abnormal current 100 ms after the Q onset was $-78°$. Current in this direction would induce a potential difference between the right and left precordial leads. Elevated potential between the right and left precordial leads has also been seen in BSPM results (BRUNS *et al.*, 2002; ECKARDT *et al.*, 2002). However, volume conduction and tissue anisotropy have non-negligible effects on the results of both MCG and BSPM. Therefore, although data gained through MCG and BSPM are not perfectly comparable, a combination of the knowledge gained through both techniques could provide new electrophysiological information on the Brugada syndome.

4.4 *Advantages of MCG in detection of the Brugada syndrome*

The MCG detected the abnormal current above the RVOT in the patients with Brugada syndrome because its spatial resolution is better than that of an ECG. In particular, cardiac mapping with sensors accurately positioned above the heart is very important in the diagnosis of the Brugada syndrome, as the weak ST elevation is only seen in a fairly small area near or in the RVOT. Furthermore, as patients with the syndrome face a relatively high risk of sudden death or ventricular tachycardia (VT), detection of the Brugada syndrome is very important, and this means we need high sensitivity and accuracy. We can expect the MCG to provide these qualities. Once we have performed a mass study of the Brugada syndrome, we may be able to detect cases with a heightened potential for fatal arrhythmia in the form of VT.

4.5 *Study limitation*

This study was limited in several ways. First, only small numbers of Brugada-syndrome ($n=6$) and CRBBB ($n=4$) patients were studied. We used the data from this small patient population as the basis for speculation on the current dispersion in Brugada-syndrome patients. Establishing the underlying mechanism and ensuring that our diagnostic method is appropriate for the syndrome will require the statistical analysis of results from large numbers of patients. Secondly, the CAM has a limitation in that it does not express the real distribution of current over the ventricular muscle; our findings may thus differ from findings based on direct measurement of the transmembrane potential. A combination of a large number of statistical CAMs, direct measurement of the transmembrane potentials in patients, and animal examination may be needed to overcome these problems. Thirdly, a consistent interpretation of the time after Q onset at which the ST-segment commences might not be possible because of the mixture of late QRS and ST-segment signals.

Although the present study is somewhat methodologically simplistic, and our results are preliminary because of the above limitations, our findings should be helpful in terms of better understanding of the mechanism and clinical implications of the Brugada syndrome.

Acknowledgments—The authors are grateful to Ito Sonoe, Syuuji Hashimoto, Norio Tanaka and Kiichi Masuda of the National Cardiovascular Center for performing the MCG measurements.

References

ANTZELEVITCH, C., BRUGADA, P., BRUGADA, J., BRUGADA, R., NADEMANEE, K., and TOWBIN, J. A. (1999): 'The Brugada syndrome', in: CAMM, J., (Ed.): 'Clinical approaches to tachyarrhythmias' (Futura Publishing Co., Armonk, NY, 1999), pp. 1–99

ANTZELEVITCH, C., BRUGADA, P., BRUGADA, J., BRUGADA, R., SHIMIZU, W., GUSSAK, I., and PEREZ-RIERA, A. R. (2002): 'Brugada syndrome: a decade of progress', *Circ. Res.*, **91**, pp. 1114–1118

BRUGADA, P., and BRUGADA, J. (1992): 'Right bundle branch block, persistent ST-segment elevation and sudden cardiac death, a distinct clinical and electrocardiographic syndrome', *J. Am. Coll. Cardiol.*, **20**, pp. 1391–1396

BRUGADA, P., BRUGADA, J., and BRUGADA, R. (2000*a*): 'The Brugada syndrome', *Ann. Noninvas. Electrocardiol.*, **5**, pp. 88–91

BRUGADA, R., BRUGADA, J., and ANTZELEVITCH, C. *et al.* (2000*b*): 'Sodium channel blockers identify risk for sudden death in patients with ST-segment elevation and right bundle branch block but structurally normal hearts', *Circulation*, **101**, pp. 510–515

BRUNS, H. J., ECKARDT, L., VAHLHAUS, C., SCHULZE-BAHR, E., HAVERKAMP, W., BORGGREFE, M., BREITHARDT, G., and WICHTER, T. (2002): 'Body surface potential mapping in patients with Brugada syndrome: right precordial ST segment variations and reverse changes in left precordial leads', *Cardiovasc. Res.*, **54**, pp. 58–66

DELGADO, C., STEINHAUS, B., DELMAR, M., CHIALVO, D. R., and JALIFE, J. (1990): 'Directional differences in excitability and margin of safety for propagation in sheep ventricular epicardial muscle', *Circ. Res.*, **67**, pp. 97–110

ECKARDT, L., BRUNS, H. J., PAUL, M., KIRCHHOF, P., SCHULZE-BAHR, E., WICHTER, T., BREITHARDT, G., BORGGREFE, M., and HAVERKAMP, W. (2002): 'Body surface area of ST elevation and the presence of late potential correlate to the inducibility of ventricular tachyarrhythmias in Brugada syndrome', *J. Cardiovasc. Electrophysiol.*, **13**, pp. 742–749

HÄMÄLINEN, M., HARI, R., ILMONIEMI, R. J., KNUUTILA, J., and LOUNASMAA, O. V. (1993): 'Magnetoencephalography—theory, instrumentation, and applications to noninvasive studies of the working human brain', *Rev. Modern Phys.*, **65**, pp. 413–497

HORIGOME, H., TSUKADA, K., KANDORI, A., SHIONO, J., MATSUI, A., TERADA, Y., and MITSUI, T. (1999): 'Visualization of regional myocardial depolarization by tangential component mapping on magnetocardiogram in children', *Int. J Cardiac Imag.*, **15**, pp. 331–337

HOSAKA, H., and COHEN, D. (1976*a*): 'Visual determination of generators of the magnetocardiogram', *J. Electrocardiol.*, **9**, pp. 426–432

HOSAKA, H., and COHEN, D. (1976*b*): 'The effects of the torso boundaries on the magnetocardiogram', *J. Electrocardiol.*, **9**, pp. 418–425

IKEDA, T. (2002): 'Brugada syndrome: current clinical aspects and risk stratification', *A. N. E.*, **7**, pp. 251–262

KANDA, M., SHIMIZU, W., MATSUO, K., NAGAYA, N., TAGUCHI, A., SUYAMA, K., KURITA, T., AIHARA, N., and KAMAKURA, S. (2002): 'Electrophysiologic characteristics and implications of induced ventricular fibrillation in symptomatic patients with Brugada syndrome', *J. Am. Coll. Cardiol.*, **39**, pp. 1799–1805

KANDORI, A., KANZAKI, H., MIYATAKE, K., HASHIMOTO, S., ITOH, S., TANAKA, N., MIYASHITA, T., and TSUKADA, K. (2001*a*): 'A method for detecting myocardial abnormality by using a total current-vector calculated from ST-segment deviation of a magnetocardiogram signal', *Med. Biol. Eng. Comput.*, **39**, pp. 21–28

KANDORI, A., KANZAKI, H., MIYATAKE, K., HASHIMOTO, S., ITOH, S., TANAKA, N., MIYASHITA, T., and TSUKADA, K. (2001*b*): 'A method for detecting myocardial abnormality by using a current-ratio map calculated from an exercise-induced magnetocardiogram', *Med. Biol. Eng. Comput.*, **39**, pp. 29–34

KANDORI, A., SHIMIZU, W., YOKOKAWA, M., MARUO, T., KANZAKI, H., NAKATANI, S., KAMAKURA, S., MIYATAKE, K., MURAKAMI, M., MIYASHITA, T., OGATA, K., and TSUKADA, K. (2002): 'Detection of spatial repolarization abnormalities in patients with LQT1 and LQT2 forms of congenital long-QT syndrome', *Physiol. Meas.*, **23**, pp. 603–614

KANZAKI, H., NAKATANI, S., KANDORI, A., TSUKADA, K., and MIYATAKE, K. (2003): 'A new screening method to diagnose coronary artery disease using multichannel magnetocardiogram and simple exercise', *Basic Res. Cardiol.*, **98**, pp. 124–132

KARINIEMI, V., AHOPELTO, J., KARP, P. J., and KATILA, T. E. (1974): 'The fetal magnetocardiogram', *J. Perinat. Med.*, pp. 214–216

KURITA, T., SHIMIZU, W., INAGAKI, M., SUYAMA, K., TAGUCHI, A., SATOMI, K., AIHARA, N., KAMAKURA, S., KOBAYASHI, J., and KOSAKAI, Y. (2002): 'The electrophysiologic mechanism of ST-segment elevation in Brugada syndrome', *J. Am. Coll. Cardiol.*, **40**, pp. 330–334

MASAKI, R., WATANABE, I., NAKAI, T., KONDO, K., OSHIKAWA, N., SUGIMURA, H., OKUBO, K., KOJIMA, T., SAITO, S., OZAWA, Y., and KANMATSUSE, K. (2002): 'Role of signal-averaged electrocardiograms for predicting the inducibility of ventricular fibrillation in the syndrome consisting of right bundle branch block and ST segment elevation in leads V1-V3', *Jpn. Heart J.*, **43**, pp. 367–378

MATSUO, K., SHIMIZU, W., KURITA, T., INAGAKI, M., AIHARA, N., and KAMAKURA, S. (1998): 'Dynamic changes of 12-lead electrocardiograms in a patient with Brugada syndrome', *J. Cardiovasc. Electrophysiol.*, **9**, pp. 74–83

MIYAZAKI, T., MITAMURA, H., MIYOSHI, S., SOEJIMA, K., AIZAWA, Y., and OGAWA, S. (1996): 'Autonomic and antiarrhythmic drug modulation of ST segment elevation in patients with Brugada syndrome', *J. Am. Coll. Cardiol.*, **27**, pp. 1061–1070

PESOLA, K., TENNER, U., NENONEN, J., ENDT, P., BRAUER, H., LEDER, U., and KATILA, T. (1999): 'Multichannel magnetocardiographic measurements with a physical thorax phantom', *Med. Biol. Eng. Comput.*, **37**, pp. 2–7

ROBERGE, F. A., VINET, A., and VICTORRI, B. (1986): 'Reconstruction of propagated electrical activity with two-dimensional model of anisotropic heart muscle', *Circ. Res.*, **58**, pp. 461–475

SATO, M., TERADA, Y., MITSUI, T., MIYASHITA, T., KANDORI, A., and TSUKADA, K. (2001): 'Detection of myocardial ischemia by magnetocardiogram using 64-channel SQUID system'. *12th Int. Congress on Biomagnetism, Biomag 2000*, pp. 523–526

SATO, M., TERADA, Y., MITSUI, T., MIYASHITA, T., KANDORI, A., and TSUKADA, K. (2002): 'Visualization of atrial excitation by magnetocardiogram', *Int. J. Cardiac Imag.*, **18**, pp. 305–312

SHIMIZU, W., ANTZELEVITCH, C., SUYAMA, K., *et al.* (2000*a*): 'Effect of sodium channel blockers on ST segment, QRS duration, and corrected QT interval in patients with Brugada syndrome', *J. Cardiovasc. Electrophysiol.*, **11**, pp. 1320–1329

SHIMIZU, W., MATSUO, K., TAKAGI, M., *et al.* (2000*b*): 'Body surface distribution and response to drugs of ST segment elevation in Brugada syndrome: clinical implication of eighty-seven-lead body surface potential mapping and its application to twelve-lead electrocardiograms', *J. Cardiovasc. Electrophysiol.*, **11**, pp. 396–404

SHIONO, J., HORIGOME, H., MATSUI, A., TERADA, Y., WATANABE, S., MIYASHITA, T., and TSUKADA, K. (2002): 'Evaluation of myocardial ischemia in Kawasaki disease using an isointegral map on magnetocardiograms', *Pacing Clin. Electrophysiol.*, **25**, pp. 915–921

TSUKADA, K., MITSUI, T., TERADA, Y., HORIGOME, H., and YAMAGUCHI, I. (1999): 'Non-invasive visualization of multiple simultaneously activated regions on torso magnetocardiographic maps during ventricular depolarization', *J. Electrocardiol.*, **32**, pp. 305–313

TSUKADA, K., MIYASHITA, T., KANDORI, A., MITSUI, T., TERADA, Y., SATO, M., SHIONO, J., HORIGOME, H., YAMADA S., and YAMAGUCHI, I. (2000*a*): 'An iso-integral mapping technique using magnetocardiogram, and its possible use for diagnosis of ischemic heart disease', *Int. J. Cardiac Imag.*, **16**, 55–66

TSUKADA, K., MIYASHITA, T., KANDORI, A., YAMADA, S., SATO, M., TERADA, Y., MITSUI, T., YAMAGUCHI, I., KANZAKI, H., KAMAKURA, S., and MIYATAKE, K. (2000*b*): 'Magnetocardiographic mapping characteristic for diagnosis of ischemic heart disease', *Comput. Cardiol.*, **27**, pp. 505–508

WILDE, A. A., ANTZELEVITCH, C., BORGGREFE, M., BRUGADA, J., BRUGADA, R., BRUGADA, P., CORRADO, D., HAUER, R. N., KASS, R. S., NADEMANEE, K., PRIORI, S. G., and TOWBIN, J. A. (2002): 'Study group on the molecular basis of arrhythmias of the European Society of cardiology: proposed diagnostic criteria for the Brugada syndrome: consensus report', *Circulation*, **106**, pp. 2514–2519

YAMADA, S., TSUKADA, K., MIYASHITA, T., NOGUCHI, Y., EBASHI, T., TERADA, Y., KUGA, K., and YAMAGUCHI, I. (2001): 'Analysis of more complex arrhythmias using the tangential components of the cardiac magnetic field'. *12th Int. Congress on Biomagnetism, Biomag 2000*, pp. 514–517

YAMADA, S., TSUKADA, K., MIYASHITA, T., OYAKE, Y., KUGA, K., and YAMAGUCHI, I. (2002): 'Noninvasive diagnosis of partial atrial standstill using magnetocardiograms', *Circ. J.*, **66**, pp. 1178–1180

YAN, G. X., and ANTZELEVITCH, C. (1999): 'Cellular basis for the Brugada syndrome and other mechanisms of arrhythmogenesis associated with ST segment elevation', *Circulation*, **100**, pp. 1660–1666

Author's biography

AKIHIKO KANDORI received the B.S. and M.S. degrees in electrical engineering from Sophia University, Tokyo, in 1988 and 1990, respectively. In 1990, he joined the Central Research Laboratory of Hitachi Ltd. From 1992 to 1994, he joined the Superconducting Sensor Laboratory of national project. He has been interested in SQUID sensor and application for many years. He received the PhD in Engineering from Sophia University, Tokyo in 1997 and a PhD in Medicine from Tsukuba University, Ibaraki in 2003. His current interests are biomagnetic imaging and SQUID sensor system.